

Spin polarization and spin-dependent scattering of holes observed in transverse magnetic focusingM. J. Rendell ^{1,*} S. D. Liles ^{2,*} A. Srinivasan ² O. Klochan ^{3,1} I. Farrer ^{4,5} D. A. Ritchie ⁵ and A. R. Hamilton ^{1,†}¹*School of Physics and Australian Research Council Centre of Excellence in Future Low-Energy Electronics Technologies, University of New South Wales, Sydney, New South Wales 2052, Australia*²*School of Physics, University of New South Wales, Sydney, New South Wales 2052, Australia*³*University of New South Wales Canberra, Canberra ACT 2600, Australia*⁴*Department of Electronic and Electrical Engineering, University of Sheffield, Sheffield S1 3JD, United Kingdom*⁵*Cavendish Laboratory, University of Cambridge, Cambridge CB3 0HE, United Kingdom*

(Received 11 October 2022; revised 15 December 2022; accepted 3 January 2023; published 12 January 2023)

In two-dimensional systems with a spin-orbit interaction, magnetic focusing can be used to create a spatial separation of particles with different spin. Here we measure hole magnetic focusing for two different magnitudes of the Rashba spin-orbit interaction. We find that when the Rashba spin-orbit magnitude is large there is significant attenuation of one of the focusing peaks, which is conventionally associated with a change in the spin polarization. We instead show that in hole systems with a k^3 spin-orbit interaction, this peak suppression is due to a change in the scattering of one spin state, not a change in spin polarization. We also show that the change in scattering length extracted from magnetic focusing is consistent with results obtained from measurements of Shubnikov–de Haas oscillations. This result suggests that scattering must be considered when relating focusing peak amplitude to spin polarization in hole systems.

DOI: [10.1103/PhysRevB.107.045304](https://doi.org/10.1103/PhysRevB.107.045304)**I. INTRODUCTION**

In a magnetic focusing experiment, a collimated beam of charge is focused by a transverse magnetic field, analogous to a mass spectrometer. Magnetic focusing was originally proposed as a method of studying the Fermi surface of metals [1,2], and has also been used to measure band structures in graphene [3], and electron-electron scattering lengths in GaAs/AlGaAs [4].

In systems with a spin-orbit interaction (SOI), the magnetic focusing trajectories become spin dependent as the spin states are now coupled to momentum. If the SOI is sufficiently large, magnetic focusing can spatially separate the spin states and create a spin-dependent mass spectrometer [5–12]. The high mobility and large SOI of two-dimensional (2D) hole systems in GaAs has made them an ideal candidate for spin-dependent magnetic focusing experiments. Experimental work has used magnetic focusing to measure spatial separation of spin [5], spin filtering by quantum point contacts (QPCs) [7], and interactions between one-dimensional subbands in a QPC [13]. Magnetic focusing of holes has also been proposed as a way to measure g -factor anisotropies [14], and complex spin dynamics [9,15], which are not visible in other measurements of 2D systems such as Shubnikov–de Haas oscillations.

Here, we concentrate on the use of magnetic focusing peak amplitude as a measure of the spin polarization [5,7,16–18]. It has been proposed that the relative amplitudes of the spin-split magnetic focusing peaks is determined by the spin

polarization of the injected charge. This technique has been used in hole systems to observe spontaneous polarization in QPC transmission [7] and spin-dependent transmission of QPCs [5,13]. Despite magnetic focusing being used for these techniques, there has been limited study of the effect of changing the magnitude of the Rashba SOI on hole magnetic focusing.

A recent study investigated magnetic focusing using a device where the Rashba SOI magnitude could be tuned *in situ* using a top gate voltage (V_{TG}) [19]. This technique revealed an increase in the spatial separation of the spin-split focusing trajectories as the Rashba SOI was increased. However, there is a limit to the amount the Rashba SOI can be changed using this method. In addition, any change to V_{TG} will also change the 2D hole density and confining potential in addition to the Rashba SOI magnitude. As such, further study requires a different method of changing the Rashba SOI.

In this work we study magnetic focusing in two lithographically identical samples which differ only in the magnitude of the Rashba SOI. We change the Rashba SOI by changing the heterostructure used to confine the 2D system, allowing us to create a large change in the magnitude of the Rashba SOI for a similar V_{TG} and 2D density. By comparing the two samples, we observe a change in the amplitude of the magnetic focusing peaks, which is typically associated with a change in the spin polarization. However, we instead find that the change in peak amplitude is consistent with an increase in scattering of one spin state rather than a change in spin polarization. We measure the scattering length of each spin state from the focusing peak amplitude, and find good agreement with scattering lengths found from Shubnikov–de Haas measurements. We conclude that the change in focusing peak amplitude is

*These authors contributed equally to this work.

†alex.hamilton@unsw.edu.au

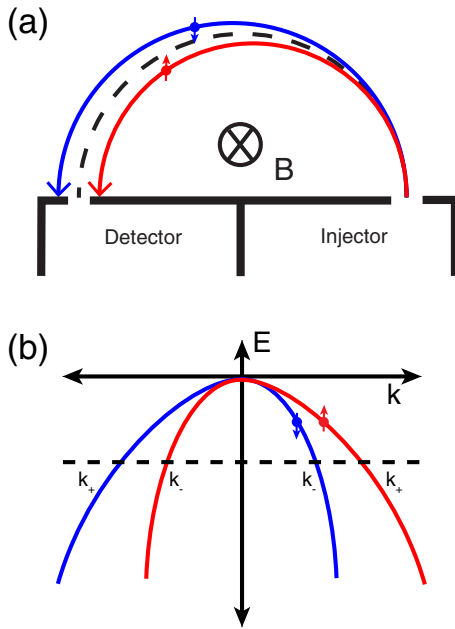


FIG. 1. (a) Magnetic focusing in the presence of a spin-orbit interaction. The red and blue lines correspond to the spin-split focusing trajectories, which result in a splitting of the first focusing peak. The dashed line corresponds to the classical focusing trajectory. (b) The first 2D subband for a hole system. Here the Rashba SOI term depends on k^3 which causes a change in the slope (and hence m^*) of the spin-resolved subbands.

due to the k^3 Rashba term causing a different effective mass and hence scattering length of each spin state, rather than a change in spin polarization. This result suggests that care must be taken when relating the amplitude of spin-split focusing peaks to the spin polarization in 2D hole systems.

II. MAGNETIC FOCUSING WITH A CUBIC RASHBA SPIN-ORBIT INTERACTION

Figure 1(a) shows a schematic of a hole magnetic focusing device. A constant current is applied through an injector, where an out-of-plane perpendicular magnetic field causes the holes to follow cyclotron orbits. The voltage across the detector is measured, and a peak is observed when the focusing diameter is equal to the spacing between injector and detector [black dashed line in Fig. 1(a)]. Peaks in the focusing signal occur when the magnetic field is an integer multiple of [20]

$$B = \frac{2\hbar k_F}{ed},$$

where k_F is the Fermi momentum and d is the distance between the injector and the collector QPC (focusing diameter). In the presence of a SOI the hole trajectories become spin dependent, resulting in a spatial separation of spin [blue and red lines in Fig. 1(a)]. The spatial spin separation causes the first magnetic focusing peak to split into two, with each peak corresponding to a different spin chirality. The relative amplitude of these spin peaks has been used as a measure of the spin polarization in 2D hole systems [5].

The form of the Rashba spin-orbit term for 2D hole systems is fundamentally different to equivalent electron systems. This difference can have a dramatic impact on spin-resolved focusing peaks. In GaAs, the subband dispersion for 2D holes with a Rashba SOI is given by [21]

$$\mathcal{E}_h = \frac{\hbar^2 k^2}{2m^*} \pm \frac{\beta E_z}{\Delta_{\text{HH-LH}}} k^3, \quad (1)$$

where E_z is the electric field in the out-of-plane direction and $\Delta_{\text{HH-LH}}$ is the splitting between the heavy hole (HH) and light hole (LH) subbands. Figure 1(b) shows the resulting HH subband dispersion for a 2D hole system with Rashba SOI. The SOI causes the momentum of the holes to become spin dependent, with two values of k (k_+ and k_-) at the Fermi energy (horizontal dashed line). In a magnetic focusing measurement, this results in separate cyclotron orbits for each spin and creates a spatial separation, splitting the first focusing peak. Previous work has demonstrated the ability to detect a change in peak splitting as the magnitude of the Rashba SOI is changed [19].

The k^3 structure of the Rashba SOI term for holes also causes the curvature of the 2D subbands to become spin dependent. This results in a difference in effective mass for each spin chirality in addition to the difference in k [22]. The spin-dependent effective mass has been used to demonstrate electrical control of the Zeeman splitting [23], and proposed as a way to detect and generate topological properties in a 2D hole system [24,25]. The change in effective mass is also possible to detect via focusing peaks. If the Rashba SOI term is sufficiently large, the difference in effective mass can be observed as a difference in scattering. Since focusing peak amplitude is exponentially sensitive to scattering [26,27], the change in effective mass will therefore impact the focusing peak amplitude. This analysis does not include contributions from k -linear Rashba SOI terms for 2D holes [28–30]. These terms do not cause a spin-dependent change in the curvature of the 2D subbands and should not affect the difference in effective mass between the spin chiralities.

III. INTERFACE DEPENDENCE

Previous studies of the Rashba SOI in hole magnetic focusing used a top gate voltage (V_{TG}) to change the Rashba SOI magnitude [19]. This technique is limited in the range of Rashba SOI magnitude that can be accessed, and also changes multiple factors of the Rashba SOI term [see Eq. (1)] as E_z , k , and $\Delta_{\text{HH-LH}}$ all depend on V_{TG} . Here we instead fix V_{TG} and create a large change in the Rashba SOI by preparing two samples with different interface symmetry. One sample uses a 15 nm (100) GaAs/ $\text{Al}_{0.33}\text{GaAs}_{0.67}$ quantum-well (QW) heterostructure with a square-well like 2D confining potential (wafer W713). The other is a (100) GaAs/ $\text{Al}_{0.33}\text{GaAs}_{0.67}$ single heterojunction (SHJ) which creates a triangular confining potential (wafer W640). Changing from a QW to a SHJ with a fixed V_{TG} reduces the 2D confinement, decreasing $\Delta_{\text{HH-LH}}$ without causing a large change in k and E_z . From Eq. (1), the SHJ device (smaller $\Delta_{\text{HH-LH}}$) will have a larger Rashba SOI term and therefore larger focusing peak splitting. The SHJ device will also have a larger difference in effective mass between the spin subbands.

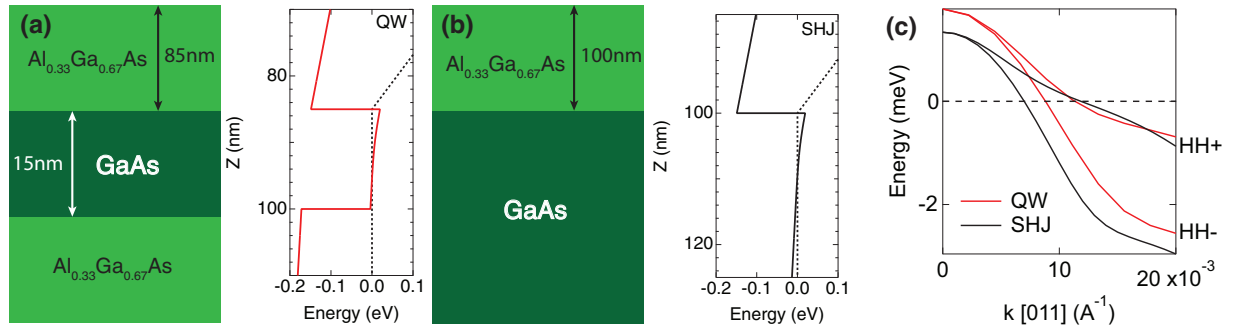


FIG. 2. Comparison of sample heterostructures. (a) Heterostructure of the QW sample and resultant band edge. (b) Heterostructure and band edge of the SHJ sample. (c) A comparison of the first HH subband dispersion for both samples. Calculated with a $6 \times 6 \mathbf{k} \cdot \mathbf{p}$ solver (NEXTNANO) at $n_{2D} = 1.5 \times 10^{11} \text{ cm}^{-2}$ (QW) and $n_{2D} = 1.92 \times 10^{11} \text{ cm}^{-2}$ (SHJ).

In order to observe clear magnetic focusing peaks, it is important to have a clean, high mobility 2D system. To achieve this, both heterostructures are undoped with an overall top gate used to induce holes in the 2D system. This results in high mobility (QW = $760\,000 \text{ cm}^{-2}/\text{V s}$ and SHJ = $600\,000 \text{ cm}^{-2}/\text{V s}$) and a long mean free path (QW = $5.3 \mu\text{m}$ and SHJ = $4.2 \mu\text{m}$) for both focusing samples. Metal split gates are used to define QPCs with lithographic dimensions of $300 \times 300 \text{ nm}$, which are used as injection and detection points for the focused holes. To minimize any influence of spin polarization [5,7] or lateral QPC biasing [11], all QPCs are biased symmetrically to the $G = 2e^2/h$ conductance plateau. All measurements are performed in a He dilution system at a base temperature of 20 mK.

Figure 2 compares the wafer structure and resultant confining potentials for the QW (a) and SHJ (b) samples. The left side of each panel is the wafer structure around the 2D interface, while the right side shows the resulting band edge found using a Schrodinger-Poisson solver (NEXTNANO [31]). The $E(k)$ dispersion relations of both samples are also calculated using NEXTNANO at a similar 2D density to the experimental data. This calculation uses a $6 \times 6 \mathbf{k} \cdot \mathbf{p}$ solver and includes contributions from Rashba SOI terms but does not include Dresselhaus SOI terms. Figure 2(c) shows the spin split first HH subbands for both samples, with a clear difference in k between the HH+ and HH- subbands at $E = 0$ (horizontal dashed line). It is this difference in k that results in a splitting of the first focusing peak in both samples.

There is a significantly larger splitting visible for the SHJ sample at E_F (horizontal dashed line), which leads to an increase in the focusing peak spacing. There is also a large difference in the curvature of the HH+ and HH- subbands. The difference in curvature of the $E(k)$ dispersion results in a spin-dependent effective mass, which can also be detected in a focusing measurement.

Figure 3 compares focusing in the QW and SHJ samples over the same focusing diameter (800 nm). Starting with the QW sample [Fig. 3(a)], we observe a clear spin-split focusing peak in positive B , with higher order peaks also observed. No splitting of higher order peaks is observed due to spin-flip reflections from the boundary [12,32]. Vertical dashed lines indicate the position of the spin-split first focusing peaks. In the opposite B polarity the holes are focused away from the

collector QPC and only Shubnikov–de Haas oscillations are visible.

The same measurement is repeated on a lithographically identical sample, fabricated on the SHJ wafer as shown in Fig. 3(b). This measurement was performed at the same V_{TG} as the QW sample, resulting in a slightly higher hole density ($n_{2D} = 1.89 \times 10^{11} \text{ cm}^{-2}$ vs $1.57 \times 10^{11} \text{ cm}^{-2}$). The increased Rashba SOI in the SHJ sample results in focusing peaks which are further apart than the QW sample. The focusing peaks in Fig. 3(b) are also significantly smaller in amplitude than those in the QW sample, with the higher field peak attenuated and broader compared to the lower field peak. Typically such a difference in amplitude of spin-resolved focusing peaks is interpreted as a change in the spin polarization [5,7]. However, here the spin polarization should be approximately equal as both QPCs are biased to the $G = 2e^2/h$ plateau to transmit both spin states.

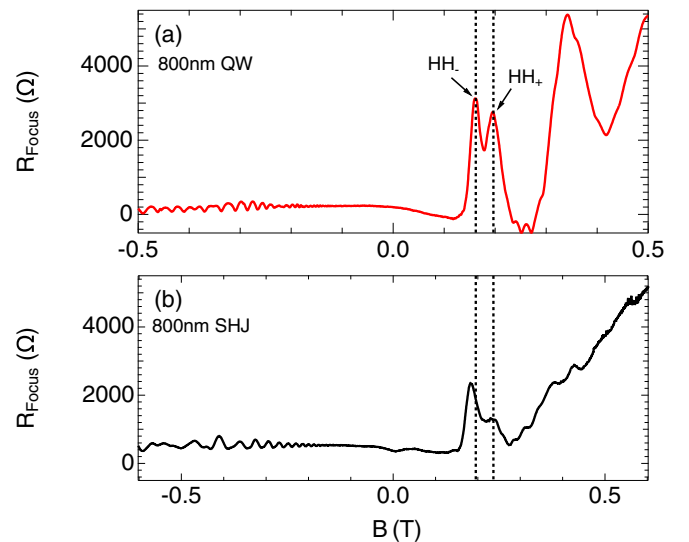


FIG. 3. Spin-split magnetic focusing with different interface symmetry. Red is focusing in a 15-nm quantum well with weaker Rashba spin orbit ($n_{2D} = 1.57 \times 10^{11} \text{ cm}^{-2}$). Black is focusing in a single heterojunction with stronger Rashba spin orbit at the same V_{TG} ($n_{2D} = 1.89 \times 10^{11} \text{ cm}^{-2}$). Dashed vertical lines indicate the spacing of the 800-nm QW focusing peaks. x axis in the bottom panel has been scaled by the ratio of n_{2D} to account for the difference in density.

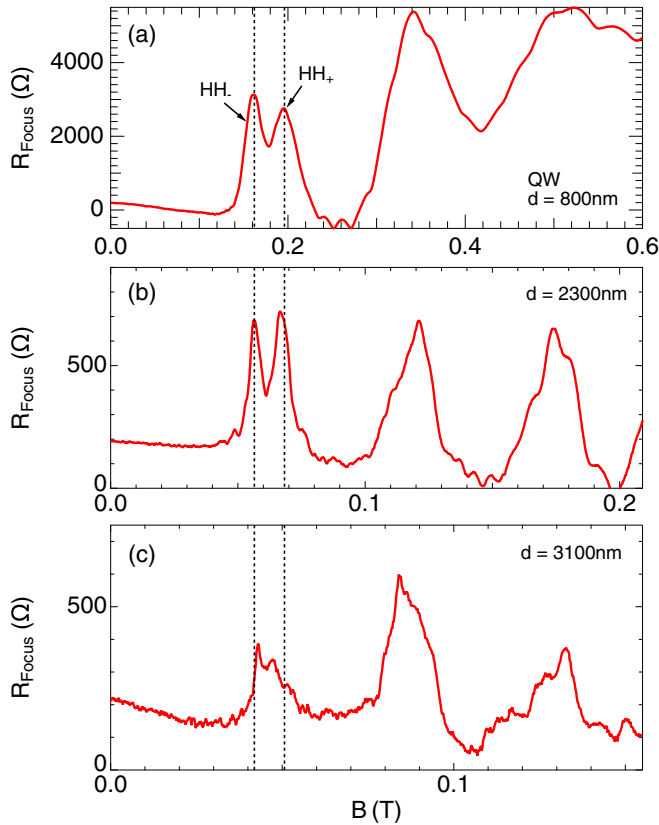


FIG. 4. Focusing over different diameters in the QW sample. The focusing diameter is varied from 800 nm (a) to 3100 nm (c). The x -axis range of each panel has been chosen based on the focusing diameter. The vertical dashed lines indicate the position of the spin-resolved focusing peaks in the 800-nm trace. Panel (a) has been reproduced from Fig. 3(a).

To determine if the change in peak amplitude in the SHJ sample is instead related to an increase in scattering, the decay of focusing peak amplitude is measured over a range of focusing diameters. The device geometry of both focusing samples allows focusing to be measured for a range of focusing diameters ($d = 800, 2300, \text{ and } 3100 \text{ nm}$). By measuring the change in peak amplitude as a function of focusing diameter, the scattering length of each of the spin peaks can be found [26,27].

First, the focusing diameter dependence of the peak amplitude is measured on the QW sample. Figure 4 shows focusing measured on the QW sample for all three focusing diameters. To allow for easy comparison between the focusing lengths, the B axis range of each plot has been chosen based on the ratio of the focusing diameters. This should result in vertical alignment of the same focusing peaks across each diameter. Vertical dashed lines indicate the position of the spin-split focusing peaks in Fig. 4(a) (focusing diameter = 800 nm). As the focusing diameter is increased from 800 nm [Fig. 4(a)] to 2300 nm [Fig. 4(b)] there is good agreement in B location between all of the peaks. Multiple higher order peaks can be observed, with the amplitude of the higher order peaks similar to the spin-split focusing peaks, indicating specular reflections from the boundary between the injector and detector QPCs. The spin-split focusing peaks can also be clearly resolved, and

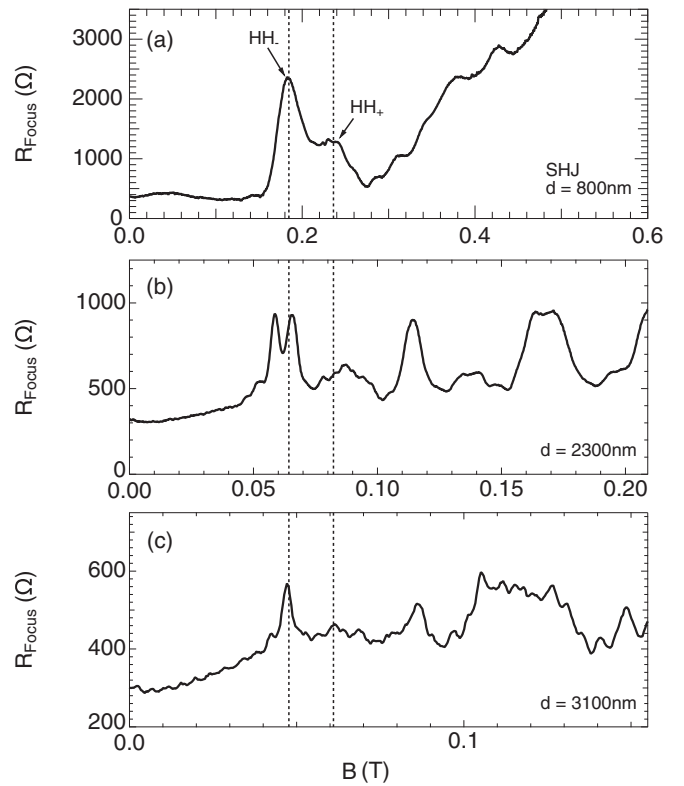


FIG. 5. Focusing comparison for the SHJ sample. Focusing over a diameter of 800 nm (a), 2300 nm (b), and 3100 nm (c). The x -axis range has been chosen to allow direct comparison of focusing peaks. Vertical dashed lines indicate the position of the spin-resolved focusing peaks for the 800-nm focusing diameter. Panel (a) has been reproduced from Fig. 3(b).

align with the peaks in Fig. 4(a) as indicated by the vertical dashed lines. The spin-split focusing peaks also have a similar amplitude, indicating an equal population of both spin states (i.e., no spin polarization). As the focusing diameter is further increased to 3100 nm [Fig. 4(c)], the effects of scattering begin to dominate the focusing signal. The amplitude of the first focusing peak is significantly reduced and both spin peaks can no longer clearly be resolved.

In Fig. 5 focusing is measured in the SHJ sample for the same three focusing diameters (800, 2300, and 3100 nm). Once again, the x -axis range of each panel has been chosen based on the focusing diameter, and the vertical dashed lines indicate the position of the spin-split focusing peaks in Fig. 5(a). The HH $-$ peak is narrow and large in amplitude, while the HH $+$ peak is significantly lower in amplitude and broader. The spacing of the peaks has also increased compared to the QW sample [Fig. 4(a)], as expected for a larger Rashba SOI magnitude. As the focusing diameter is increased from 800 nm [Fig. 5(a)] to 2300 nm [Fig. 5(b)], multiple changes can be observed. First, the amplitude of all focusing peaks decreases with the increase in focusing path length. In particular, the HH $+$ spin peak becomes very broad and low in amplitude. In comparison, the HH $-$ spin-split peak is higher in amplitude and narrower, and both spin peaks have superimposed interference structure as the QPC width

is of the same order as the Fermi wavelength ($\lambda_F \simeq 60$ nm) [12,20,33,34]. The HH $-$ spin peak displays a structure similar to a spin-split focusing peak; however, this splitting is too small to be caused by spin. The structure on the HH $-$ peak is most likely due to an interference effect, as similar (but smaller amplitude) oscillations are visible on the low B side of the peak, a characteristic signature of interference due to diffraction in focusing [12,34]. Finally, as the focusing diameter is increased to 3100 nm [Fig. 5(c)] the amplitude of the HH $+$ and HH $-$ peaks is further reduced, with the HH $+$ peak barely resolved due to scattering.

The significantly lower amplitude of the HH $+$ spin-split peak in Fig. 5 is consistent with the larger effective mass of this spin band [see Fig. 2(c)]. Assuming the scattering time is the same, the larger effective mass should result in a shorter scattering length for the HH $+$ spin state. As the total path length traveled by both spin states is the same, being fixed by the focusing geometry, a shorter scattering length will result in more scattering for the HH $+$ state and hence a lower amplitude of the corresponding HH $+$ focusing peak. Since focusing measurements are exponentially sensitive to scattering effects [26,27,35], a change in scattering rate can be the dominant cause of the amplitude change, rather than a change in the spin polarization. In induced GaAs 2D hole systems, this scattering is typically caused by background impurities and interface roughness [36,37], as there are no intentional dopants to cause additional scattering.

IV. SCATTERING LENGTH

To understand the suppression of the HH $+$ peak in the SHJ focusing sample, we extract the scattering length of both spin peaks and compare this to the scattering length extracted from Shubnikov–de Haas oscillations. The amplitude of focusing peaks decays exponentially as the focusing path length is increased:

$$R_{\text{Focus}} \propto Ae^{-\pi d/2l}, \quad (2)$$

where l is the small-angle scattering length [26,27,35] and d is the focusing diameter. By fitting a double Gaussian to the spin peaks for each focusing diameter, the amplitude of the peaks can be found as a function of path length.

Figures 6(a)–6(c) show the results of a double Gaussian fit to the SHJ focusing peaks for all focusing lengths. The amplitude of the spin-split peaks as a function of focusing path length is plotted on the semilogarithmic axes in Fig. 6(d). A straight line fit to the data in Fig. 6(d) allows the scattering length for each of the spin peaks to be found (l_+ and l_-). It is difficult to directly compare the scattering lengths found from focusing to a mean free path for two reasons. First, focusing measurements require the holes to travel through a narrow detector QPC, where even small scattering events can be sufficient to prevent a hole from reaching the detector. Second, the value of the scattering length found from focusing is sensitive to the choice of background resistance used for the peak fitting. However, the ratio of the scattering lengths is independent of the background resistance. From the linear fits in Fig. 6(d), Eq. (2) can be used to find the scattering length for each spin state (l_+ and l_-). From this we find that $l_+/l_- = 0.77 \pm 0.01$.

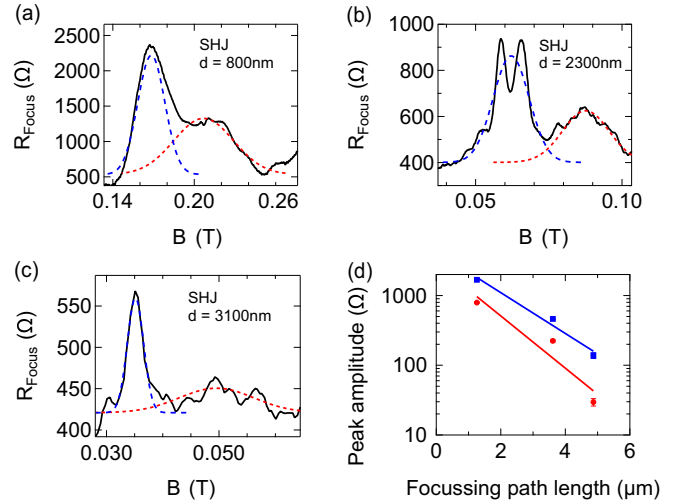


FIG. 6. Focusing decay length for the SHJ sample. (a)–(c) Gaussian fits to the spin-split focusing peaks on the SHJ sample for all focusing diameters. (d) Fit to the amplitude of each spin peak with error bars showing the fit uncertainty. From this we can obtain the scattering length for each spin.

Finally, the ratio of the scattering lengths is compared to a ratio found from Shubnikov–de Haas oscillations. The scattering length is given by $l \propto v_F \tau$, where τ is the scattering time. Assuming that τ is constant for both spin states, the ratio of v_F (i.e., v_+/v_-) can be used to predict the ratio of l_+/l_- . The ratio of v_+/v_- can be found from the ratio of the densities of the spin states (n_+/n_-) since

$$\frac{v_+}{v_-} = \frac{n_+ m_-}{m_+ n_-} = \frac{k_+ m_-}{k_- m_+}.$$

Assuming the subbands are approximately parabolic this expression can be simplified to

$$\frac{l_+}{l_-} = \frac{v_+}{v_-} = \sqrt{\frac{n_-}{n_+}}.$$

The values of n_+ and n_- were found from measurements of the frequency of Shubnikov–de Haas oscillations on the same sample ($f = nh/e$). From this $n_+ = 1.21 \times 10^{11} \text{ cm}^{-2}$ and $n_- = 0.68 \times 10^{11} \text{ cm}^{-2}$ which gives a predicted ratio of $l_+/l_- = 0.75$, almost identical to the measured value of $l_+/l_- = 0.76$.

The good agreement between the predicted and measured ratios of l indicates that the increased scattering of one spin state is the likely cause of the difference in peak amplitude observed in the SHJ focusing sample.

There are some potential limitations of the scattering analysis in this work. The assumption of equal scattering times between the spin states may not be adequate, depending on the difference in m^* . Previous calculations of the effects of scattering in GaAs hole systems show some dependence on the effective mass [36,37]; however, these do not consider the effects of multiple spin subbands. Extending these calculations to multiple subbands is possible [38] but is outside the scope of this work. Additionally, in this work we have only considered effects of the Rashba spin-orbit interaction. This technique could also be extended to other k^3 spin-orbit terms

such as those caused by Dresselhaus spin-orbit interactions. While these terms are expected to be small in (100) GaAs [39], comparison with focusing in less symmetric heterostructures [such as (311) GaAs] may allow for contributions from Dresselhaus spin-orbit interactions to be extracted from focusing.

V. CONCLUSIONS

In this work we have investigated magnetic focusing with a large change in the magnitude of the Rashba spin-orbit interaction. We observed an attenuation of one of the spin peaks that is typically associated with a change in spin polarization. Here we have instead shown that the difference in peak amplitude is consistent with a difference in effective mass and hence scattering rate between the spin chiralities.

This result indicates that care must be taken when associating the amplitude of focusing peaks to spin polarization in hole systems with k^3 spin-orbit interaction.

ACKNOWLEDGMENTS

The authors would like to thank S. Bladwell, O. P. Sushkov, E. Y. Sherman, and U. Zülicke for many valuable discussions. Devices were fabricated at the UNSW node of the Australian National Fabrication Facility (ANFF). This research was funded by the Australian Government through the Australian Research Council Discovery Project Scheme; Australian Research Council Centre of Excellence FLEET (Project No. CE170100039); and by the UK Engineering and Physical Sciences Research Council (Grant No. EP/R029075/1).

-
- [1] Y. Sharvin, A possible method for studying Fermi surfaces, *Sov. J. Exp. Theor. Phys.* **48**, 984 (1965).
- [2] V. Tsoi, Focusing of electrons in a metal by a transverse magnetic field, *ZhETF Pis. Red.* **19**, 114 (1974) [*Sov. J. Exp. Theor. Phys.* **19**, 114 (1974)].
- [3] T. Taychatanapat, K. Watanabe, T. Taniguchi, and P. Jarillo-Herrero, Electrically tunable transverse magnetic focusing in graphene, *Nat. Phys.* **9**, 225 (2013).
- [4] A. Gupta, J. J. Heremans, G. Kataria, M. Chandra, S. Fallahi, G. C. Gardner, and M. J. Manfra, Precision measurement of electron-electron scattering in GaAs/AlGaAs using transverse magnetic focusing, *Nat. Commun.* **12**, 5048 (2021).
- [5] L. P. Rokhinson, V. Larkina, Y. B. Lyanda-Geller, L. N. Pfeiffer, and K. W. West, Spin Separation in Cyclotron Motion, *Phys. Rev. Lett.* **93**, 146601 (2004).
- [6] A. Dedigama, D. Deen, S. Murphy, N. Goel, J. Keay, M. Santos, K. Suzuki, S. Miyashita, and Y. Hirayama, Current focusing in InSb heterostructures, *Phys. E (Amsterdam, Neth.)* **34**, 647 (2006).
- [7] L. P. Rokhinson, L. N. Pfeiffer, and K. W. West, Spontaneous Spin Polarization in Quantum Point Contacts, *Phys. Rev. Lett.* **96**, 156602 (2006).
- [8] J. Heremans, H. Chen, M. Santos, N. Goel, W. Van Roy, and G. Borghs, Spin-dependent transverse magnetic focusing in InSb and InAs-based heterostructures, *AIP Conf. Proc. No. 893* (AIP, Melville, NY, 2007), p. 1287.
- [9] U. Zülicke, J. Bolte, and R. Winkler, Magnetic focusing of charge carriers from spin-split bands: Semiclassics of a Zitterbewegung effect, *New J. Phys.* **9**, 355 (2007).
- [10] S. Bladwell and O. P. Sushkov, Magnetic focusing of electrons and holes in the presence of spin-orbit interactions, *Phys. Rev. B* **92**, 235416 (2015).
- [11] S.-T. Lo, C.-H. Chen, J.-C. Fan, L. W. Smith, G. L. Creeth, C.-W. Chang, M. Pepper, J. P. Griffiths, I. Farrer, H. E. Beere, G. A. C. Jones, D. A. Ritchie, and T.-M. Chen, Controlled spatial separation of spins and coherent dynamics in spin-orbit-coupled nanostructures, *Nat. Commun.* **8**, 15997 (2017).
- [12] Y. K. Lee, J. S. Smith, and J. H. Cole, Influence of device geometry and imperfections on the interpretation of transverse magnetic focusing experiments, *Nanoscale Res. Lett.* **17**, 31 (2022).
- [13] S. Chesi, G. F. Giuliani, L. P. Rokhinson, L. N. Pfeiffer, and K. W. West, Anomalous Spin-Resolved Point-Contact Transmission of Holes due to Cubic Rashba Spin-Orbit Coupling, *Phys. Rev. Lett.* **106**, 236601 (2011).
- [14] S. Bladwell and O. P. Sushkov, Measuring hole g -factor anisotropies using transverse magnetic focusing, *Phys. Rev. B* **99**, 081401(R) (2019).
- [15] S. Bladwell and O. P. Sushkov, Interference in spin-orbit coupled transverse magnetic focusing: Emergent phase due to in-plane magnetic fields, *Phys. Rev. B* **98**, 085438 (2018).
- [16] R. M. Potok, J. A. Folk, C. M. Marcus, and V. Umansky, Detecting Spin-Polarized Currents in Ballistic Nanostructures, *Phys. Rev. Lett.* **89**, 266602 (2002).
- [17] J. A. Folk, R. M. Potok, C. M. Marcus, and V. Umansky, A gate-controlled bidirectional spin filter using quantum coherence, *Science* **299**, 679 (2003).
- [18] T. M. Chen, M. Pepper, I. Farrer, G. A. C. Jones, and D. A. Ritchie, All-Electrical Injection and Detection of a Spin-Polarized Current Using 1D Conductors, *Phys. Rev. Lett.* **109**, 177202 (2012).
- [19] M. J. Rendell, S. D. Liles, A. Srinivasan, O. Klochan, I. Farrer, D. A. Ritchie, and A. R. Hamilton, Gate voltage dependent Rashba spin splitting in hole transverse magnetic focusing, *Phys. Rev. B* **105**, 245305 (2022).
- [20] H. van Houten, C. W. J. Beenakker, J. G. Williamson, M. E. I. Broekaart, P. H. M. van Loosdrecht, B. J. van Wees, J. E. Mooij, C. T. Foxon, and J. J. Harris, Coherent electron focusing with quantum point contacts in a two-dimensional electron gas, *Phys. Rev. B* **39**, 8556 (1989).
- [21] R. Winkler, *Spin-Orbit Coupling Effects in Two-Dimensional Electron and Hole Systems* (Springer-Verlag, Berlin, Heidelberg, 2003).
- [22] H. L. Stormer, Z. Schlesinger, A. Chang, D. C. Tsui, A. C. Gossard, and W. Wiegmann, Energy Structure and Quantized Hall Effect of Two-Dimensional Holes, *Phys. Rev. Lett.* **51**, 126 (1983).
- [23] E. Marcellina, A. Srinivasan, D. S. Miserev, A. F. Croxall, D. A. Ritchie, I. Farrer, O. P. Sushkov, Dimitrie Culcer, and A. R. Hamilton, Electrical Control of the Zeeman Spin Splitting in Two-Dimensional Hole Systems, *Phys. Rev. Lett.* **121**, 077701 (2018).
- [24] E. Marcellina, P. Bhalla, A. R. Hamilton, and D. Culcer, Signatures of quantum mechanical Zeeman effect in classical transport due to topological properties of two-dimensional spin- $\frac{3}{2}$ holes, *Phys. Rev. B* **101**, 121302(R) (2020).

- [25] J. H. Cullen, P. Bhalla, E. Marcellina, A. R. Hamilton, and D. Culcer, Generating a Topological Anomalous Hall Effect in a Nonmagnetic Conductor: An In-Plane Magnetic Field as a Direct Probe of the Berry Curvature, *Phys. Rev. Lett.* **126**, 256601 (2021).
- [26] J. Heremans, M. Santos, and M. Shayegan, Observation of magnetic focusing in two-dimensional hole systems, *Appl. Phys. Lett.* **61**, 1652 (1992).
- [27] M. Rendell, O. Klochan, A. Srinivasan, I. Farrer, D. Ritchie, and A. Hamilton, Transverse magnetic focussing of heavy holes in a (100) GaAs quantum well, *Semicond. Sci. Technol.* **30**, 102001 (2015).
- [28] E. Rashba and E. Sherman, Spin-orbital band splitting in symmetric quantum wells, *Phys. Lett. A* **129**, 175 (1988).
- [29] J.-W. Luo, A. N. Chantis, M. van Schilfhaarde, G. Bester, and A. Zunger, Discovery of a Novel Linear-in- k Spin Splitting for Holes in the 2D GaAs/AlAs System, *Phys. Rev. Lett.* **104**, 066405 (2010).
- [30] M. V. Durnev, M. M. Glazov, and E. L. Ivchenko, Spin-orbit splitting of valence subbands in semiconductor nanostructures, *Phys. Rev. B* **89**, 075430 (2014).
- [31] <http://www.nextnano.de/>.
- [32] A. A. Reynoso, G. Usaj, and C. A. Balseiro, Magnetic breakdown of cyclotron orbits in systems with Rashba and Dresselhaus spin-orbit coupling, *Phys. Rev. B* **78**, 115312 (2008).
- [33] K. Aidala, R. Parrott, T. Kramer, E. Heller, R. Westervelt, M. Hanson, and A. Gossard, Imaging magnetic focusing of coherent electron waves, *Nat. Phys.* **3**, 464 (2007).
- [34] S. Bladwell and O. P. Sushkov, Interference effects and Huygens principle in transverse magnetic focusing of electrons and holes, *Phys. Rev. B* **96**, 035413 (2017).
- [35] J. Spector, H. Stormer, K. Baldwin, L. Pfeiffer, and K. West, Ballistic electron transport beyond 100 μm in 2D electron systems, *Surf. Sci.* **228**, 283 (1990).
- [36] J. C. H. Chen, D. Q. Wang, O. Klochan, A. P. Micolich, K. Das Gupta, F. Sfigakis, D. A. Ritchie, D. Reuter, A. D. Wieck, and A. R. Hamilton, Fabrication and characterization of ambipolar devices on an undoped AlGaAs/GaAs heterostructure, *Appl. Phys. Lett.* **100**, 052101 (2012).
- [37] D. Q. Wang, J. C. H. Chen, O. Klochan, K. Das Gupta, D. Reuter, A. D. Wieck, D. A. Ritchie, and A. R. Hamilton, Influence of surface states on quantum and transport lifetimes in high-quality undoped heterostructures, *Phys. Rev. B* **87**, 195313 (2013).
- [38] M. Y. Simmons, A. R. Hamilton, S. J. Stevens, D. A. Ritchie, M. Pepper, and A. Kurobe, Fabrication of high mobility *in situ* back-gated (311)A hole gas heterojunctions, *Appl. Phys. Lett.* **70**, 2750 (1997).
- [39] A. Srinivasan, D. S. Miserev, K. L. Hudson, O. Klochan, K. Muraki, Y. Hirayama, D. Reuter, A. D. Wieck, O. P. Sushkov, and A. R. Hamilton, Detection and Control of Spin-Orbit Interactions in a GaAs Hole Quantum Point Contact, *Phys. Rev. Lett.* **118**, 146801 (2017).